Chapter 3

FLOW LIQUEFACTION INSTABILITY AS A MECHANISM FOR LOWER END OF LIQUEFACTION CHARTS

[1] U. Mital, T. Mohammadnejad, and J.E. Andrade. "Flow liquefaction instability as a mechanism for lower end of liquefaction charts". submitted. 2016.

3.1 Introduction

The state-of-the-practice uses the "simplified procedure" [71] for evaluating liquefaction susceptibility of soils. Based on this procedure, liquefaction charts have been developed that correlate soil resistance to earthquake-induced stresses. Laboratory studies typically quantify soil resistance in terms of void ratio or relative density. On the other hand, field studies typically resort to Standard Penetration Test (SPT), Cone Penetration Test (CPT), or shear wave velocity (V_S) measurements to quantify soil resistance. As pointed out by Dobry and Abdoun [24], this creates a disconnect between laboratory and field measurements. Moreover, liquefaction charts are inherently empirical in nature since they have been developed using case histories. Therefore, there is a poor understanding regarding the underlying physics of these charts, which makes extrapolation into regimes with insufficient case history data difficult. To get the most out of liquefaction charts, it is vital that research be carried out to incorporate more physics in these charts [33]. Studies have been conducted in the past (for example, [9, 10, 24, 33, 78, 79]) to bridge the gap between physics and empiricism. This paper seeks to take another step in that direction.

One of the criticisms of liquefaction charts is that although they give useful information regarding triggering of liquefaction, they do not inform an engineer about the effects of liquefaction [24]. In this paper, we hypothesize that the lower end of liquefaction charts corresponds to unstable flow liquefaction. This informs us about the mechanism of liquefaction at the site, and helps us understand the effects of liquefaction at the lower end of liquefaction charts. In the following sections, we start by reviewing a prevailing explanation about the mechanics of the liquefaction charts [24]. Based on this explanation, we will formulate our hypothesis. Finally, we will present some results of our numerical investigation supporting our hypothesis.

3.2 Background

Recently, Dobry and Abdoun [24] proposed an explanation for the mechanics of the entire liquefaction curve. They proposed that liquefaction charts are essentially a combination of curves of increasing cyclic shear strain (γ_c). If a soil is subjected to N_c cycles of cyclic shear strain greater than γ_c, pore pressure develops leading to liquefaction. The lower end corresponds to normally consolidated sand (K_0 = 0.5) with $\gamma_c \approx$ 0.03-0.05%. The explanation for the upper end is more speculative. It is proposed to correspond to overconsolidated (K_0 = 0.75-1.0), preshaken, and geologically aged sands for which $\gamma_c \approx$ 0.1-0.3%. Note that the requisite cyclic shear strain γ_c for the upper end is approximately 10 times that for the lower end. This is because the pore pressure build-up is much smaller for the upper end. The aforementioned quantities correspond to an earthquake magnitude of M_w = 7 (for which N_c = 10 [71]), and an effective initial confining pressure of p'_0 = 50 kPa. Figure 3.1 presents a summary.

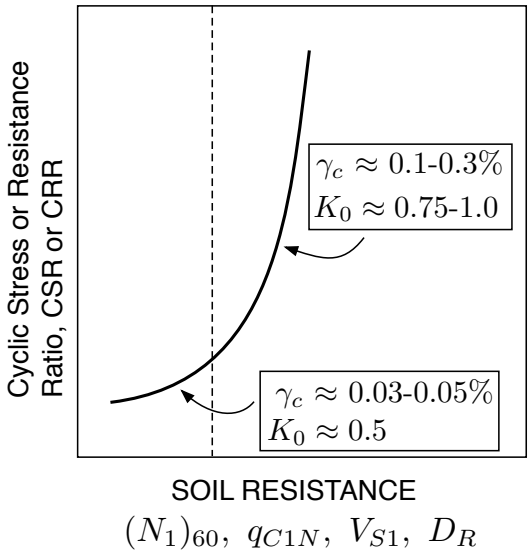

Figure 3.1: Summary of explanation of liquefaction charts as proposed by Dobry and Abdoun [24]. This corresponds to the earthquake magnitude M_w= 7 and the effective initial confining pressure, p'_0 = 50 kPa. Soil resistance can be quantified using either normalized SPT resistance $(N_1)_{60}$, normalized CPT tip resistance q_{C1N}, normalized shear wave velocity V_{S1}, or relative density D_R. The loading experienced by the soil is quantified using the cyclic stress ratio (CSR).

In a triaxial setting, the loading experienced by the soil is quantified using the cyclic stress ratio (CSR), defined as:

$$\text{CSR} = \frac{q_{\text{cyc}}}{2p'_0} \tag{3.1}$$

where q_{cyc} is the the magnitude of uniform cyclic deviatoric stress imposed on the soil sample, and p'_0 is the initial confining pressure. Furthermore, the cyclic stress ratio that is just enough for soil to liquefy is called the cyclic resistance ratio (CRR). The deviatoric stress may be defined as $q = \sigma'_1 - \sigma'_3$, while the confining pressure may be defined as $p' = (\sigma'_1 + 2\sigma'_3)/3$. σ'_1 and σ'_3 are the effective axial and radial stresses, respectively. Note that the initial confining pressure may be either isotropic or anisotropic.

3.3 Mechanics of liquefaction charts

Based on the explanation proposed by Dobry and Abdoun [24], we hypothesize that the lower end of liquefaction charts corresponds to sites that are susceptible to flow liquefaction; while the upper end corresponds to sites susceptible to cyclic mobility. To understand this better, it would be useful to review the definitions of flow liquefaction and cyclic mobility.

Flow liquefaction is an instability that can be triggered at small strains when the applied shear stress is greater than the residual or the steady state strength of the soil [44, 79]. Assuming incompressibility of pore water and undrained loading conditions, the stress path eventually reaches a peak value. Instability is triggered when the soil is loaded beyond the peak of the stress path [44]. This peak also coincides with the vanishing of second order work [31]; under the constraints of undrained loading, that is equivalent to the hardening modulus reaching a limiting value [3, 4], as well as vanishing of the liquefaction matrix [61]. Once instability is triggered, the unstable soil loses strength and undergoes large deformations (Figure 3.2). The confining pressure drops, but may or may not drop all the way to zero.

Cyclic mobility, on the other hand, can occur when the applied shear stress is lower than the residual or the steady state strength of soil [44, 79]. It involves progressive degradation of shear stiffness as the effective pressure drops with each load cycle, leading to accumulation of strains. Unlike flow liquefaction instability, there is no clear-cut point at which cyclic mobility initiates [44]. The strain accumulation seems to accelerate once the effective stress path reaches the steady state line [44, 79]. An empirical criterion to mark the onset of liquefaction (regardless of it being flow liquefaction or cyclic mobility) is the attainment of 3% shear strain [34]. In this work, we will use the 3% strain criterion to mark the onset of cyclic mobility.

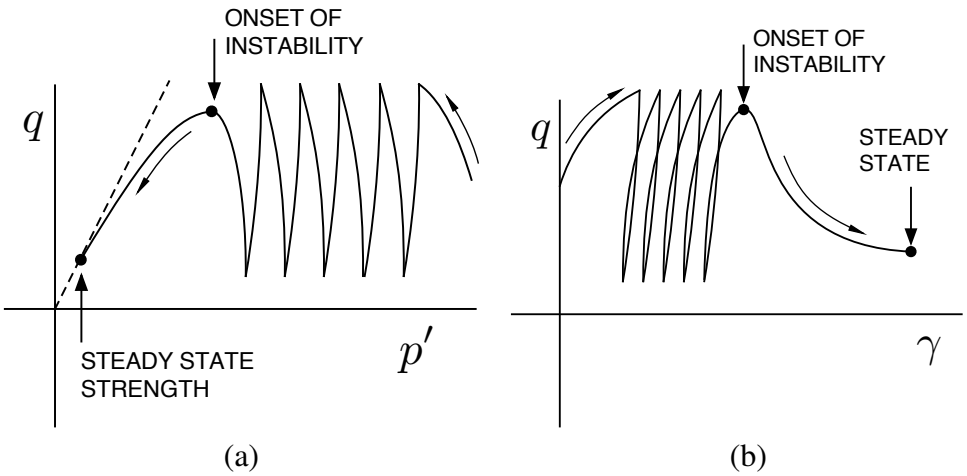

Figure 3.2: Schematic for flow liquefaction during cyclic loading (a): Effective stress path (q vs p'). (b) Shear stress (q) vs shear strain (γ). The dashed line represents the steady state line. Note that the applied shear stress is greater than the steady state strength.

Figure 3.3 shows schematic diagrams of the cyclic mobility phenomenon.

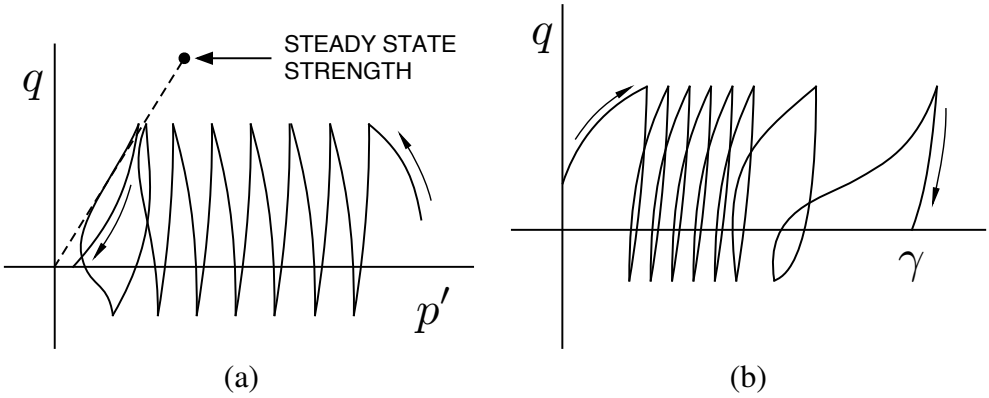

Figure 3.3: Schematic for cyclic mobility during cyclic loading (a): Effective stress path (q vs p'). (b) Shear stress (q) vs shear strain (γ). The dashed line represents the steady state line. Note that the applied shear stress is lower than the steady state strength.

It is important to note that the mechanics of strain accumulation are different for flow liquefaction and cyclic mobility. In the case of flow liquefaction, strains start accumulating rapidly after the onset of instability [44]. After instability, the assembly liquefies of its own accord, following a monotonic path without the need for any external loading. Failure is sudden, signifying a high pore pressure build-up. However, in the case of cyclic mobility, even though strains start accumulating more

intensely once the the stress path reaches the steady state line, the strain accumulation is not as intense as during flow liquefaction. The assembly does *not* lose shear strength and become unstable. It needs to be continually subjected to cyclic loading to cause further strain accumulation. If there is stress reversal, the confining pressure may drop to zero. If there is no stress reversal, the stress path simply moves up and down the steady state line [44]. Significant strains may develop over time with a more gradual pore pressure build-up. Note that the shear strain corresponding to steady state in the flow liquefaction case (Figure 3.2) is much larger than the final shear strain shown in the cyclic mobility case (Figure 3.3). However, for the sake of clarity, the difference in their magnitudes has not been highlighted.

Various experimental results show that onset of flow liquefaction instability occurs at values of shear strain lower than 3% (for instance, [14, 37, 76, 81, 86]), which is the empirical strain criterion used to mark the onset of liquefaction[34]. Given that the lower end of liquefaction charts has been proposed to correspond to sites that liquefy at lower values of strain, it seems plausible that the lower end of liquefaction charts corresponds to sites susceptible to unstable flow liquefaction. Similarly, since the upper end of the charts has been proposed to correspond to sites that liquefy at higher values of strains due to a much smaller pore pressure build-up, it seems plausible that the upper end of liquefaction charts corresponds to sites susceptible to cyclic mobility. Figure 3.4 summarizes the proposed hypothesis. In the remaining part of the paper, we numerically investigate the lower end of a relative density based liquefaction chart and also simulate the effect of static shear on a loose soil. These simulations help provide support to our hypothesis.

Liquefaction charts as a function of relative density

Liquefaction charts were first proposed as a function of relative density [72]. Since then, a number of factors other than relative density have been found to be important in evaluating liquefaction resistance. Nevertheless, charts based on relative density still provide valuable insight into liquefaction resistance. It has been pointed out that for recently deposited, normally consolidated, and non-preshaken sands, relative density is strongly correlated to normalized penetration and shear wave velocity values [24]. Since the lower end of liquefaction charts corresponds to normally consolidated sands, relative density can adequately quantify liquefaction resistance of soils corresponding to the lower end of liquefaction charts (for a given soil structure or fabric). In this paper, we use relative density to quantify soil resistance at

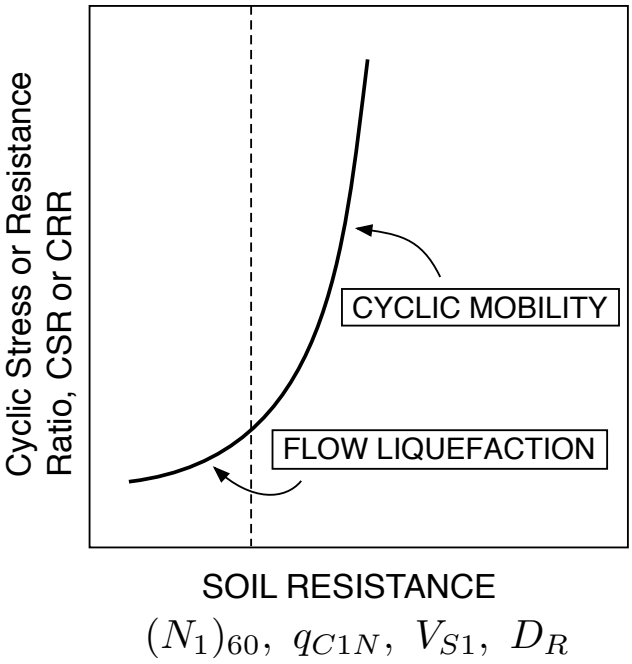

Figure 3.4: Proposed hypothesis. The lower end of liquefaction charts corresponds to flow liquefaction, while the upper end corresponds to cyclic mobility.

the lower end of liquefaction charts.

3.4 Numerical simulations of undrained cyclic triaxial test

We numerically simulated liquefaction in an undrained cyclic triaxial test, using the Dafalias-Manzari plasticity model [18]. The implementation details can be found in [61]. By successively varying the relative density of our numerical soil sample, we obtained a liquefaction chart as a function of relative density. The lower end of the chart was found to correspond to flow liquefaction, which was marked by onset of instability [3, 4, 31, 61]. The upper end did not exhibit unstable behavior and hence the 3% strain criterion was used to flag cyclic mobility [34]. The simulated chart is qualitatively similar to the one obtained by Seed and Peacock [72].

Model calibration

Table 3.1 outlines the parameters used in the Dafalias-Manzari plasticity model [18]. For a brief description of the model parameters, refer to Appendix A. We calibrated the model to some experiments on Ottawa Sand, carried out by Vaid and Chern [79]. Figures 3.5 and 3.6 show some of their results, along with the corre-

sponding simulations which served to calibrate the model. Figure 3.5 corresponds to monotonic loading. The monotonic simulations capture a very important aspect of the experiment, namely the peaking of the stress path in loose sands and phase transformation behavior in the dense sand. Moreover, the location of the steady state line in simulations is very similar to that in experiments. Figure 3.6 corresponds to a cyclic loading experiment. The cyclic simulation captures two important aspects of the experiment. Firstly, flow liquefaction is initiated following the peak in the stress path, which occurs in the 8th cycle. Secondly, the cyclic stress ratio (CSR) (Section 3.2) is the same as that in the experiment. Vaid and Chern [79] expressed their results in a slightly different format and defined CSR as the ratio $(\sigma'_1 - \sigma'_3)/2\sigma'_{3c}$, where σ'_1 and σ'_3 are as defined in Section 3.2 and σ'_{3c} is the initial radial stress. Figure 3.6 uses the definition used by Vaid and Chern [79].

Constant	Variable	Value
Elasticity	G_0	125
	ν	0.05
Critical State	M	1.45
	λ_c	0.065
	e_0	0.722
	ξ	0.9
Yield surface	m	0.01
Plastic modulus	h_0	4.5
	c_h	1.05
	n^b	1.1
Dilatancy	A_0	0.124
	n^d	5.5
Fabric-dilatancy tensor	$z_{\max}$	4
	c_z	600

Table 3.1: Parameters for the Dafalias Manzari Constitutive Model

Simulating the liquefaction chart

In order to simulate the liquefaction chart, each sample had an initial pressure of 100 kPa, and was subjected to 10 loading cycles. Ten loading cycles approximately correspond to an earthquake of magnitude $M_w = 7$ [71]. As discussed in section 3.3, flow liquefaction was deemed to have initiated when the stress path peaked. This also coincides with the vanishing of second order work [31], the hardening modulus reaching a limiting value [3, 4], as well vanishing of the liquefaction matrix [61]. If the stress path did not peak, the cyclic stress ratio (CSR) resulting in 3%

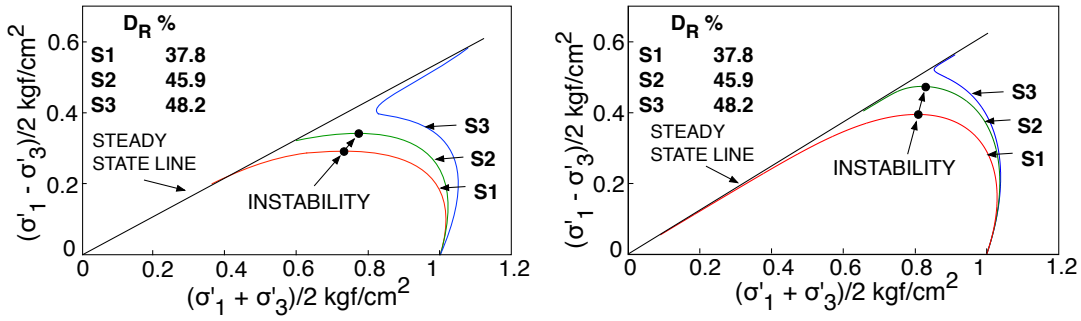

(a) (b)

Figure 3.5: Calibration results for monotonic loading stress paths: (a) Experiments [79]; (b) Simulations

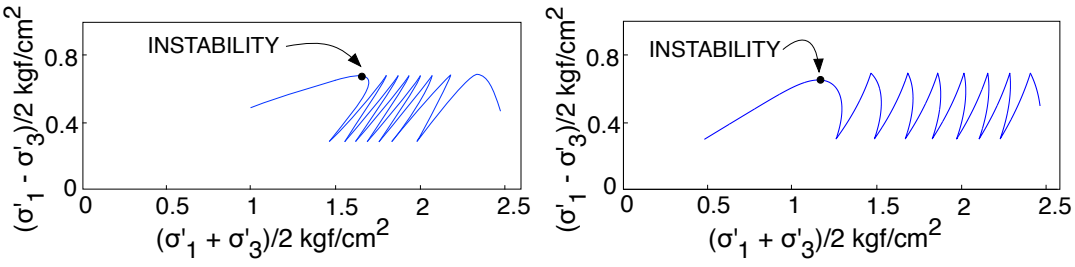

(a) (b)

Figure 3.6: Calibration results for cyclic loading stress path: (a) Experiment [79]; (b) Simulation. The relative density of the soil is 42.8% and CSR is 0.094.

strain [34] was recorded. By successively varying the relative density of the numerical samples, and recording the approporiate CSR, we obtained a liquefaction chart. We picked $K_0 = 0.5$ in order to simulate normally consolidated sand. We picked relative densities over a range of about 30% - 80%. Relative densities lower than a critical value—$D_{R(crit)}$—exhibited unstable flow liquefaction (Figure 3.7). Higher densities made the soil susceptible to cyclic mobility (Figure 3.8). Figure 3.9 shows the liquefaction chart obtained using our simulations, where the lower end ($D_R < D_{R(crit)}$) corresponds to flow liquefaction. In our simulations, $D_{R(crit)}$ was approximately 43%. It may be noted that, qualitatively, this chart is similar to the one proposed by Seed and Peacock [72].

Remark: We would like to point out that although the critical relative density value $D_{R(crit)} \approx 43\%$ forms the boundary between the lower and upper end of the liquefaction chart obtained using our simulations, it should not be taken as a bound-

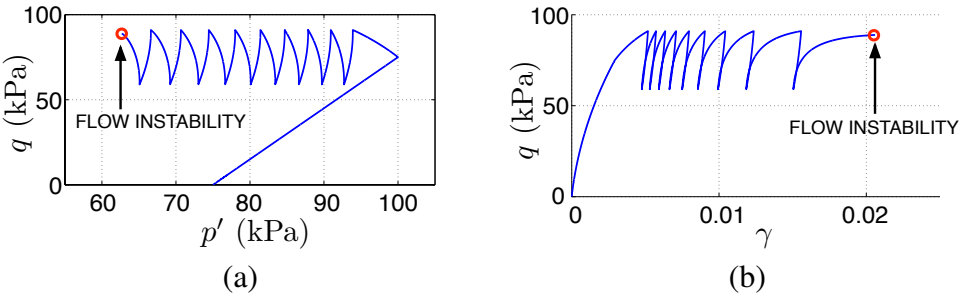

Figure 3.7: (a): Effective stress path for D_R = 42%. (b): Stress-strain path for D_R = 42%. Flow liquefaction instability [4, 31, 61] occurs in the 10th cycle, in this case at a little over 2% strain.

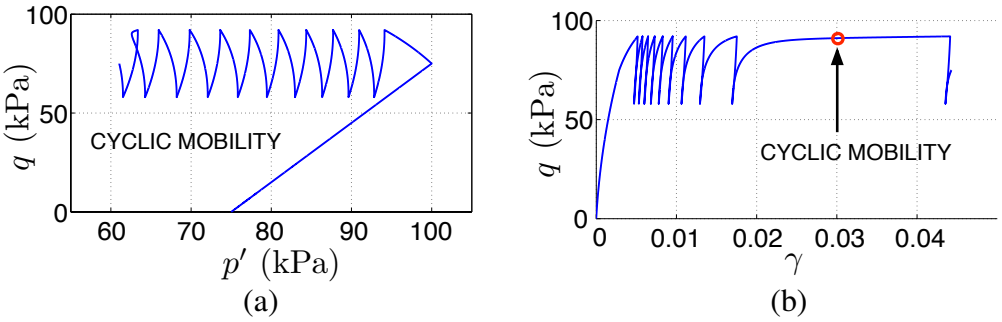

Figure 3.8: (a) Effective stress path for D_R = 44%. (b): Stress-strain path for D_R = 44%. Sample does not become unstable although large strains start accumulating. Onset of cyclic mobility as signified by 3% shear strain occurs in the 10th cycle.

ary between the lower and upper end of liquefaction charts in general. For D_R-based charts, the boundary may vary depending on factors such as the initial stress state, stress history, and fabric of the sand. For the present set of simulations, $D_{R(crit)} \approx$ 43% seems consistent with the experiments to which the model was calibrated[79]. For V_S-based charts, the boundary between lower and upper end may be taken from the study by Dobry and Abdoun [24]. For clean sands, this boundary corresponds to $V_{S1} \approx 160$ m/s. For SPT and CPT-based charts, appropriate correlations developed by Andrus et al. [6] may be used. For clean sands, these may be given by $(N_1)_{60} \approx 15$ and $q_{c1N} \approx 80$.

Simulating effect of static shear stress

Simulating the effect of static shear on a loose soil helps us understand why soils at the lower end of liquefaction charts may be susceptible to unstable flow liquefaction. The effect of static shear is usually quantified by a static shear correction

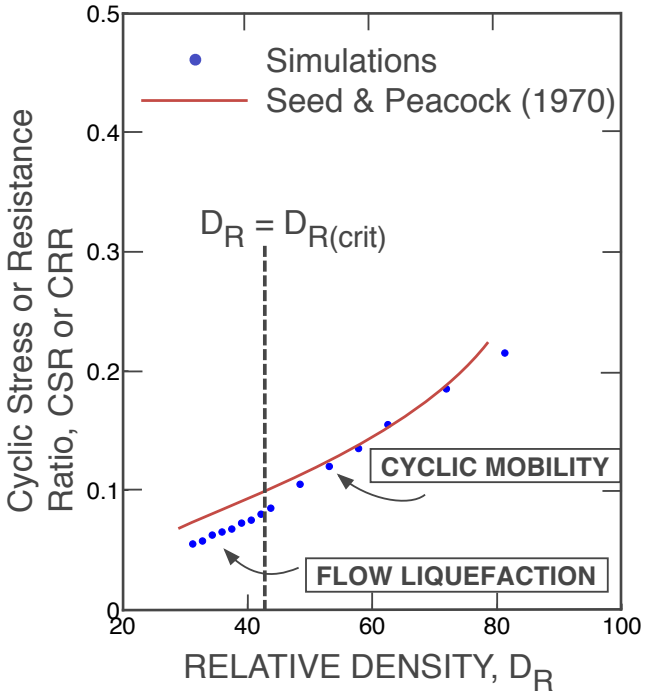

Figure 3.9: Simulated liquefaction chart as a function of relative density; comparison with the Seed and Peacock curve [72]. The critical relative density $D_{R(crit)}$ separates the chart into a lower and an upper end.

factor K_α, which is defined as:

$$K_\alpha = \frac{\text{CRR}}{\text{CRR}_{\alpha=0}} \tag{3.2}$$

Here, $\alpha = q_s/2p'_0$, where q_s and p'_0 are the values of static shear and effective confining pressure, respectively, at the beginning of cyclic loading. CRR is the cyclic resistance ratio. It is the CSR that is just enough to cause liquefaction. CRR in the numerator is the value associated with the actual value of α, while CRR in the denominator is the value associated with $\alpha = 0$ (isotropic stress state). As will soon become evident, the liquefaction chart simulated in Figure 3.9 corresponds to $\alpha = 0.375$.

We reproduced a K_α curve (Figure 3.10) for $D_R = 35\%$ under a confining pressure of 100 kPa. This relative density corresponds to the lower end of D_R-based liquefaction chart (Figure 3.9). We obtained a trend similar to the one in the literature for soils with low liquefaction resistance [11, 34, 73].

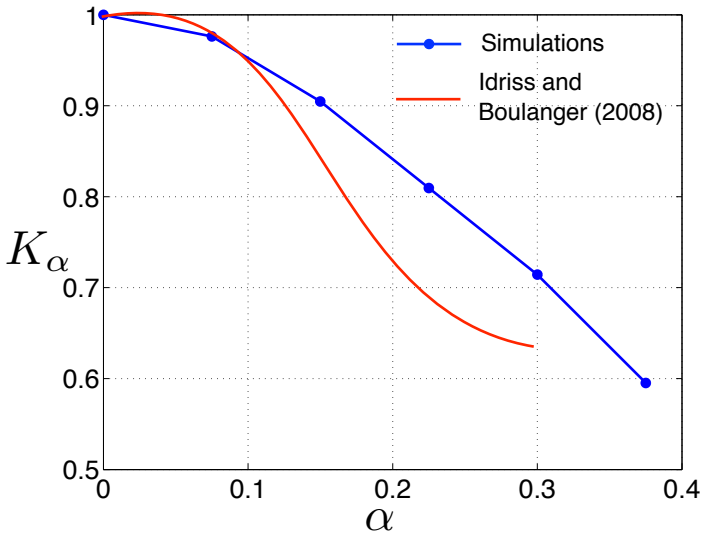

Figure 3.10: Simulated K_α curve for a loose soil ($D_R = 35\%$) corresponding to the lower end of relative density liquefaction chart; comparison with the curve proposed by Boulanger [34]

For the set of simulations in Figure 3.10, α varied from 0 to 0.375. For $\alpha = 0$, the soil exhibited cyclic mobility. For the remaining initial states, the soil was susceptible to flow liquefaction. As pointed out by Vaid and Chern [78, 79], with increasing static shear, loose sands become more susceptible to liquefaction. This can be easily understood using the concept of instability line [78, 79] and collapse envelope [2]. As the quantity of static shear increases, the initial state of the sample moves closer to the instability line, making it more susceptible to flow liquefaction (Figure 3.11).

Figure 3.10 can also be interpreted in terms of the coefficient of earth pressure at rest, or K_0. In a triaxial test, K_0 can be defined as:

$$K_0 = \frac{\sigma'_{30}}{\sigma'_{10}} \tag{3.3}$$

where σ'_{30} is the effective radial stress and σ'_{10} is the effective axial stress prior to undrained loading. It can be shown that in a triaxial test, K_0 and α are related as:

$$K_0 = \frac{3 - 2\alpha}{3 + 4\alpha} \tag{3.4}$$

Physically, $0 < K_0 \leq 1$. Within this range, it can be checked that an increase in α implies a reduction in K_0. This implies that lower values of K_0 make a loose

soil more susceptible to flow liquefaction, due to increasing proximity of the initial stress state to the instability line. Specifically, $\alpha = 0.375$ corresponds to $K_0 = 0.5$, which is the coefficient of earth pressure for normally consolidated sand. This implies that a normally consolidated loose soil has an initial stress state that is close to the instability line. Recall that the lower end of liquefaction charts has been proposed to correspond to normally consolidated soils (Section 3.2). Furthermore, as discussed in section 3.3, the lower end of liquefaction charts corresponds to soils with a low relative density, i.e., loose soils. Therefore, Figures 3.10 and 3.11 give further credence to the hypothesis that the lower end of liquefaction charts represent loose soils susceptible to flow liquefaction.

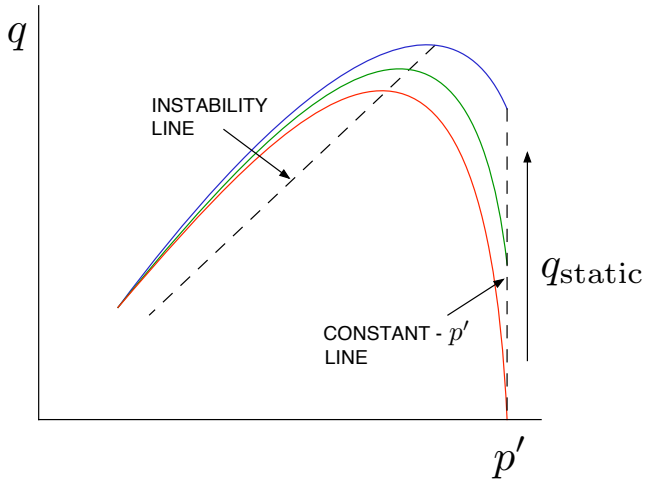

Figure 3.11: Effective stress state diagram for simulating effect of static shear stress. The monotonic stress paths serve as approximate envelopes for cyclic loading stress paths [2]. Note that as the static shear stress (q_{static}) increases, the initial state of the soil moves closer to the instability line.

3.5 Conclusions

The results of our numerical simulations suggest that sites corresponding to the lower end of liquefaction charts are susceptible to flow liquefaction instability. We used relative density to quantify soil resistance. The use of relative density is justified as there is a strong correlation between relative density and penetration values for normally consolidated sands. As proposed by Dobry and Abdoun [24], the lower end of liquefaction charts corresponds to sites that are composed of normally consolidated sands. The work presented in this paper provides additional insight regarding the effects of liquefaction at sites corresponding to the lower end of liquefaction charts. It should be noted that our numerical investigation does not conclusively validate the occurrence of cyclic mobility at the upper end of liquefac-

tion charts, since relative density is not sufficient to estimate liquefaction behavior in that regime. The critical relative density that separates a chart into a lower and an upper end is likely a function of factors like initial stress state, geological and seismic history, and the fabric of sands. A deeper understanding of how such factors affect the critical relative density can provide further insight into the physical mechanism that affects the critical relative density. Regarding sites corresponding to the lower end of liquefaction charts, liquefaction will occur as a consequence of an instability, which will lead to loss of soil strength and large deformations. This is in contrast with cyclic mobility behavior where liquefaction is a consequence of progressive degradation in shear stiffness; soil does not lose stability. As a result, if a site corresponds to the lower end of liquefaction charts, an engineer can estimate not only the loading needed to trigger liquefaction, but also gain some insight regarding the effects of liquefaction. For instance, it could be useful in augmenting the procedure for calculating the 'Liquefaction Potential Index' (LPI), as defined by Iwasaki et al [38]. LPI is used in estimating the severity of liquefaction manifestation at the ground surface. A modification could be foreseen where a higher weight could be used while calculating LPI, if the site in question is susceptible to flow liquefaction. This would result in a higher value of LPI, which would imply a greater severity of liquefaction manifestation at the ground surface.

In summary, the overlying objective of this paper was to take another step towards bridging the gap between physics and empiricism when it comes to using liquefaction charts. The work presented in this paper represents an important step towards integrating the states of art and practice.